14. I. Barman, C. R. Kong, G. P. Singh, R. R. Dasari, and M. S. Feld, "Accurate spectroscopic calibration for noninvasive glucose monitoring by modeling the physiological glucose dynamics," Anal. Chem. **82**(14), 6104–6114 (2010).
15. J. L. Lambert, C. C. Pelletier, and M. Borchert, "Glucose determination in human aqueous humor with Raman spectroscopy," J. Biomed. Opt. **10**(3), 031110 (2005).
16. R. Marbach, T. Koschinsky, F. A. Gries, and H. M. Heise, "Noninvasive blood glucose assay by near-infrared diffuse reflectance spectroscopy of the human inner lip," Appl. Spectrosc. **47**(7), 875–881 (1993).
17. K. Maruo, M. Tsurugi, M. Tamura, and Y. Ozaki, "In vivo noninvasive measurement of blood glucose by near-infrared diffuse-reflectance spectroscopy," Appl. Spectrosc. **57**(10), 1236–1244 (2003).
18. C. Vrančić, A. Fomichova, N. Gretz, C. Herrmann, S. Neudecker, A. Pucci, and W. Petrich, "Continuous glucose monitoring by means of mid-infrared transmission laser spectroscopy in vitro," Analyst (Lond.) **136**(6), 1192–1198 (2011).
19. I. Gabriely, R. Wozniak, M. Mevorach, J. Kaplan, Y. Aharon, and H. Shamoon, "Transcutaneous glucose measurement using near-infrared spectroscopy during hypoglycemia," Diabetes Care **22**(12), 2026–2032 (1999).
20. C. D. Malchoff, K. Shoukri, J. I. Landau, and J. M. Buchert, "A novel noninvasive blood glucose monitor," Diabetes Care **25**(12), 2268–2275 (2002).
21. P. Zheng, C. E. Kramer, C. W. Barnes, J. R. Braig, and B. B. Sterling, "Noninvasive glucose determination by oscillating thermal gradient spectrometry," Diabetes Technol. Ther. **2**(1), 17–25 (2000).
22. R. Ballerstadt, C. Evans, A. Gowda, and R. McNichols, "In vivo performance evaluation of a transdermal near-infrared fluorescence resonance energy transfer affinity sensor for continuous glucose monitoring," Diabetes Technol. Ther. **8**(3), 296–311 (2006).
23. W. March, D. Lazzaro, and S. Rastogi, "Fluorescent measurement in the non-invasive contact lens glucose sensor," Diabetes Technol. Ther. **8**(3), 312–317 (2006).
24. J. Kottmann, J. M. Rey, J. Luginbühl, E. Reichmann, and M. W. Sigrist, "Glucose sensing in human epidermis using mid-infrared photoacoustic detection," Biomed. Opt. Express **3**(4), 667–680 (2012).
25. G. Spanner and R. NieBner, "New concept for the non-invasive determination of physiological glucose concentrations using modulated laser diodes," Fresenius J. Anal. Chem. **354**, 327–328 (1996).
26. G. B. Christison and H. A. MacKenzie, "Laser photoacoustic determination of physiological glucose concentrations in human whole blood," Med. Biol. Eng. Comput. **31**(3), 284–290 (1993).
27. C. J. Pouchert, *The Aldrich Library of Infrared Spectra* (Aldrich Chemical Co., ed. 3, 1981).
28. H. A. MacKenzie, H. S. Ashton, S. Spiers, Y. Shen, S. S. Freeborn, J. Hannigan, J. Lindberg, and P. Rae, "Advances in photoacoustic noninvasive glucose testing," Clin. Chem. **45**(9), 1587–1595 (1999).
29. W. B. Martin, S. Mirov, and R. Venugopalan, "Using two discrete frequencies within the middle infrared to quantitatively determine glucose in serum," J. Biomed. Opt. **7**(4), 613–617 (2002).
30. W. B. Martin, S. Mirov, and R. Venugopalan, "Middle infrared, quantum cascade laser optoelectronic absorption system for monitoring glucose in serum," Appl. Spectrosc. **59**(7), 881–884 (2005).
31. X. Guo, A. Mandelis, A. Matvienko, K. Sivagurunathan, and B. Zinman, "Wavelength-modulated differential laser photothermal radiometry for blood glucose measurements," J. Phys.: Confer. Ser. **214**, 012025 (2010).
32. X. Guo, A. Mandelis, and B. Zinman, "Non-invasive glucose measurements using wavelength modulated differential photothermal radiometry (WM-DPTR)," Int. J. Thermophys., doi:10.1007/s10765-012-1276-z.
33. A. Mandelis and X. Guo, "Method of performing wavelength modulated differential laser photothermal radiometry with high sensitivity," U. S. patent application No. 20110118571 (Nov. 17, 2010).
34. A. Mandelis and X. Guo, "Wavelength-modulated differential photothermal radiometry: theory and experimental applications to glucose detection in water," Phys. Rev. E Stat. Nonlin. Soft Matter Phys. **84**(4), 041917 (2011).
35. X. Guo, A. Mandelis, and B. Zinman, "Applications of ultrasensitive wavelength-modulated differential photothermal radiometry to noninvasive glucose detection in blood serum," J. Biophotonics, http://onlinelibrary.wiley.com/doi/10.1002/jbio.201200103/abstract.
36. K. J. Wientjes and A. J. Schoonen, "Determination of time delay between blood and interstitial adipose tissue glucose concentration change by microdialysis in healthy volunteers," Int. J. Artif. Organs **24**(12), 884–889 (2001).
37. P. J. Stout, N. Peled, B. J. Erickson, M. E. Hilgers, J. R. Racchini, and T. B. Hoegh, "Comparison of glucose levels in dermal interstitial fluid and finger capillary blood," Diabetes Technol. Ther. **3**(1), 81–90 (2001).
38. I. Barman, C. R. Kong, N. C. Dingari, R. R. Dasari, and M. S. Feld, "Development of robust calibration models using support vector machines for spectroscopic monitoring of blood glucose," Anal. Chem. **82**(23), 9719–9726 (2010).
39. A. C. Guyton and J. E. Hall, *Textbook of Medical Physiology* (W.B. Saunders Co. Philadelphia, PA, 1996), pp 971–983.
40. U. Werner, K. Giese, B. Sennhenn, K. Plamann, and K. Kölmel, "Measurement of the thermal diffusivity of human epidermis by studying thermal wave propagation," Phys. Med. Biol. **37**(1), 21–35 (1992).
41. A. M. Stoll, *Heat Transfer in Biotechnology*, Vol 4 of Advances in Heat Transfer, J. P. Hartnett and T. Irvin, eds. (New York, Academic, 1967), p 117.
42. Pranalytica Inc, Daylight Solutions, personal communication (2012).

1. Introduction

Diabetes is widespread nowadays. Over 300 million people in the world are affected. The great impact of diabetes on human health includes the potential damage to heart, blood

#173338 - $15.00 USD Received 26 Jul 2012; revised 14 Oct 2012; accepted 23 Oct 2012; pub. 29 Oct 2012

vessels, eyes, kidneys and nerves over time. For proper management of diabetes, self-monitoring of blood glucose (SMBG) is required for all insulin-treated patients with diabetes [1,2]. The current SMBG approaches recommended by the American Diabetes Association are invasive (finger-pricking) [3] or minimally invasive (embedded in skin) [4]. However, the discomfort and inconvenience of the approaches lead to poor compliance with the required SMBG frequency (at least 3 times a day) [2]. A noninvasive device for determining blood glucose would permit more frequent testing and therefore a tighter control of the disease.

For more than two decades researchers have been exploring techniques which could measure blood glucose noninvasively. Despite some encouraging results and great efforts made over the past years, there is still no noninvasive device available at present for use in clinical practice [1,2]. Among all the noninvasive glucose monitoring attempts, optical methods are the most promising [5–11]. Active research areas have included polarimetry [12,13], Raman spectroscopy [14,15], diffuse reflection spectroscopy [16,17], absorption/transmission spectroscopy [18,19], thermal emission spectroscopy [20,21], fluorescence spectroscopy [22,23] and photoacoustic spectroscopy [24–26]. The spectral range of highest interest has been the near infrared (NIR) because of the relatively low water absorption and hence the deeper optical penetration into blood vessels [5,7,8]. However, the feasibility of NIR methods is strongly hindered by weak glucose absorption bands (overtone and combination bands) and confounding bands from other blood constituents. In contrast, the mid-infrared (MIR) region involves a prominent glucose absorption band which is peaked at ca. 9.7 μm [27], and is isolated from other interfering peaks in human blood [21,25,26,28–30]. Difficulties in the MIR range are the strong water absorption and the resulting background fluctuation for single-ended and contact methods. The absorption method [29,30] is limited by the small optical path. Photoacoustic methods [24,26,28] and the thermal radiation method [20,21], are suffering from water baseline variation interference (water accumulation) due to the intrinsically contacting nature of these techniques.

Recently we developed a noninvasive and noncontacting technique, wavelength modulated differential laser photothermal radiometry (WM-DPTR) for continuous or intermittent glucose monitoring in the MIR range [31–35]. In the mid-infrared range (8.5μm – 10.5 μm) where WM-DPTR operates, non-glucose-specific tissue absorption and scattering are minimal, while they are common difficulties in the visible and near infrared regions. We have demonstrated the high glucose sensitivity of WM-DPRT in water-glucose mixture [31,32,34] and serum-glucose mixture [35] measurements in the physiological concentration range. In this paper we extend the application of WM-DPTR to the measurement of serum-glucose in human skin in vitro, which is a crucial pre-clinical phase step.

2. WM-DPTR principle and signal generation

The WM- DPTR method consists of out-of-phase modulated laser-beam excitation at two discrete wavelengths near the peak (~9.5 μm) and the baseline (~10.4 μm) of the mid-infrared glucose absorption band as shown in Fig. 1. Two quantum cascade lasers (QCL) are used, resulting in differential blackbody emission detected via a HgCdZnTe (MCZT) detector (2–5 μm spectral detection bandwidth) as a photothermal up-conversion process. The differential method suppresses the strong background signal due to water absorption while the narrow detector spectral bandwidth eliminates source-detector interference, thus greatly enhancing glucose detection sensitivity. Because of the shallow penetration depth in the MIR range, WM-DPTR is designed to measure glucose concentration in the interstitial fluid (ISF) in the epidermis layer within 100 μm from the surface, which is correlated to blood glucose concentration with ~10 minutes delay [36]. However, variances in the reported lag time between ISF and blood glucose concentration, range from 0 to 45 minutes. Stout *et al* [37] reported an average 25 minutes lag in diabetes patients. For intermittent glucose measurements, the lag may have an impact on measurement accuracy. To overcome this, Barman *et al* [38] developed an algorithm that relates the two concentrations and allows predicting blood glucose levels from the glucose concentration in interstitial fluid. For

#173338 - $15.00 USD Received 26 Jul 2012; revised 14 Oct 2012; accepted 23 Oct 2012; pub. 29 Oct 2012

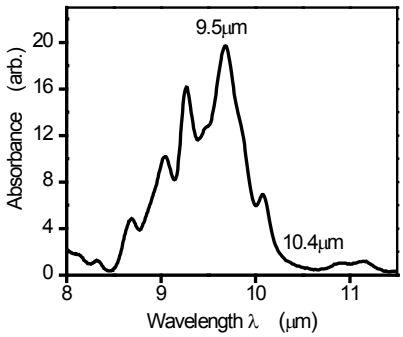

Fig. 1. FTIR glucose absorption spectrum in the MIR range from aqueous glucose solutions with water absorption baseline subtracted.

continuous glucose measurements the more important aspects are the trend and rate of glucose concentration change at a given time, not the absolute value of glucose concentration.

The theoretical model of the WM-DPTR is based on differential photothermal radiometric signal generation following sequential optical absorption of two out-of-phase square-wave modulated laser beams by a semi-infinite one-dimensional medium [34]. The PTR signal generated by a single laser is as follows:

$$S_j(t) = \Delta Q_j(t) = \left[\frac{\bar{\mu}_{IR} K(\lambda_1,\lambda_2)\alpha}{2k}\right] I_{0j}\mu_{ej}\tau_{tj} \left\{ \begin{array}{l} \dfrac{1}{\bar{\mu}_{IR}+\mu_{ej}}\left[W\left(\sqrt{\dfrac{t}{\tau_{tj}}}\right)+W\left(\sqrt{\dfrac{t}{\tau_{IR}}}\right)-2\right] \\ +\dfrac{1}{\bar{\mu}_{IR}-\mu_{ej}}\left[W\left(\sqrt{\dfrac{t}{\tau_{tj}}}\right)-W\left(\sqrt{\dfrac{t}{\tau_{IR}}}\right)\right] \\ +\dfrac{2}{\bar{\mu}_{IR}}\left\{2\sqrt{\dfrac{t}{\pi\tau_{tj}}}-\sqrt{\dfrac{\tau_{IR}}{\tau_{tj}}}\left[1-W\left(\sqrt{\dfrac{t}{\tau_{IR}}}\right)\right]\right\} \end{array} \right\}; j = A, B \tag{1}$$

where $\bar{\mu}_{IR}$ is the spectrally-weighted IR absorption/emission coefficient for homogeneous absorbers, $K(\lambda_1,\lambda_2)$ is a factor related to the detector collection bandwidth $[\lambda_1,\lambda_2]$, α and k are thermal diffusivity and thermal conductivity of the medium, respectively, I_{0j} is laser beam intensity ($j = A, B$ indicates laser A or laser B), μ_{ej} denotes optical absorption coefficient, $\tau_{tj} \equiv 1/\mu_{ej}^2\alpha$ is a photothermal time constant indicating heat conduction in the photo-excited medium from a distance equal to the optical absorption depth, $W(x) \equiv e^{x^2} erfc(x)$, and $\tau_{IR} \equiv 1/\alpha\bar{\mu}_{IR}^2$ is a photothermal time constant indicating conductive heat transfer from a length equal to the mean infrared optical absorption depth, $1/\bar{\mu}_{IR}$.

Over the full square optical waveform repetition period $0 \le t \le \tau_0$, the sequence of photothermal responses is as follows:

$$S_{AB}(t) = \begin{cases} \Delta Q_A(t); \qquad 0 \le t \le \dfrac{\tau_0}{2} \ \text{(laser A on; laser B off)} \\ \Delta Q_A(t) - \Delta Q_A\left(t-\dfrac{\tau_0}{2}\right) + \Delta Q_B\left(t-\dfrac{\tau_0}{2}\right); \quad \dfrac{\tau_0}{2} \le t \le \tau_0 \ \text{(laser A off; laser B on)} \end{cases} \tag{2}$$

#173338 - $15.00 USD Received 26 Jul 2012; revised 14 Oct 2012; accepted 23 Oct 2012; pub. 29 Oct 2012

For WM-DPTR with lock-in detection, which is the case in this study, the demodulated WM-DPTR signal at the fundamental angular frequency $\omega_0 = 2\pi/\tau_0$ is described by amplitude A_{AB} and phase P_{AB} :

$$A_{AB} = \sqrt{\Delta S_{IP}{}^2 + \Delta S_Q{}^2},\ P_{AB} = \tan^{-1}\left(\frac{\Delta S_Q}{\Delta S_{IP}}\right) \tag{3}$$

where $\Delta S_{IP}(\omega_0) = 2b_1(\omega_0)/\pi$ is in-phase and $\Delta S_Q(\omega_0) = -2a_1(\omega_0)/\pi$ is quadrature signal with

$$\begin{bmatrix} a_1(\omega_0) \\ b_1(\omega_0) \end{bmatrix} = \frac{\omega_0}{\pi}\int_0^{\tau_0} S_{AB}(t)\begin{bmatrix} \cos(\omega_0 t) \\ \sin(\omega_0 t) \end{bmatrix} dt \tag{4}$$

3. WM-DPTR system and materials

3.1. WM-DPTR system

An experimental WM-DPTR system was developed as shown in Fig. 2. The system consists of two quantum cascade lasers (QCL, 1101-95/104-CW-100-AC, Pranalytica, CA) emitting at 9.5 μm and 10.4 μm, a HgCdZnTe detector (MCZT, PVI-4TE-5, Vigo Systems, Poland) sensitive in the 2-5 μm spectral bandwidth, a function generator (33220A, Agilent Technologies, CA) generating two phase-locked square waves to modulate the laser beams,and a lock-in amplifier (SR850, Stanford Research Systems, CA). When the two out-of-phase square-wave-modulated laser beams irradiate the sample, a differential PTR signal is generated. The signal is collected by the MCZT detector and then sent to the lock-in amplifier for demodulation through a pair of parabolic mirrors. The intensity ratio of the two lasers is controlled by a motorized variable circular neutral density filter (Reynard Corp, CA) placed in front of laser B and the phase difference between the two laser beams is sensitively controlled by the phase-locked function generator. Both laser output powers are approximately 35 mW with beam sizes ~2.5 mm. The current laser power density is higher than the maximum permissible exposure (MPE) for human skin (100 mW/cm^2) at the above working wavelengths. With more stable QC lasers, and thus higher signal-to-noise ratio, the power density can be reduced to the skin safe level. To simulate glucose detection in ISF in epidermis, the laser modulation frequency which controls the WM-DPTR probing depth was set at 90 Hz in order to generate a probe depth < 40 μm in the epidermis layer (~60% water) below the ~10-μm-thick stratum corneum (~10% water).

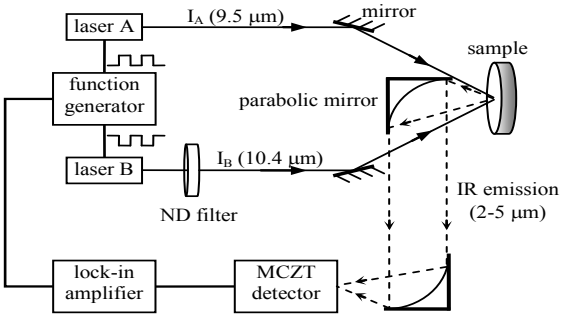

Fig. 2. WM-DPTR system setup for glucose measurements. Square-wave modulated radiation from laser A (9.5 μm) and laser B (10.4 μm) co-incident on the sample generate superposed IR emissions. The differential infrared photon flux is collected by the MCZT detector acting as a band pass filter (2-5 μm, dashed line) and sent to a lock-in amplifier. The function generator controls the phase shift between the two laser beams, and the variable circular neutral density (ND) filter controls the intensity ratio of the two lasers I_A/I_B.

#173338 - $15.00 USD Received 26 Jul 2012; revised 14 Oct 2012; accepted 23 Oct 2012; pub. 29 Oct 2012

3.2. Materials

Serum-glucose mixtures were obtained by dissolving D-glucose in glucose-depleted base human serum (1016011, American Biological Technologies Inc. TX) with glucose concentrations ~25 mg/dl (pure serum) - 280 mg/dl. Accurate glucose concentrations of the mixtures were determined using a biochemistry analyzer (YSI 2700S, Life Sciences, OH). The glucose detection range was chosen to monitor both hyperglycemia and hypoglycemia, the two problematic ranges in diabetes blood glucose regulation. Human serum was chosen because it is a good alternative for ISF [39]. The sample solution was contained in a cylindrical cell (R-10-22, International Crystal Laboratories, NJ) with human skin on one side facing the laser beams and a ZnSe window on the other side, as indicated in Fig. 3.

With the approval of the Research Ethics Office of the University of Toronto, human abdomen skin samples were obtained from abdominal plastic surgery ("tummy tuck" procedure) at the Toronto Institute of Aesthetic Plastic Surgery. The freshly harvested human skin with hypodermis layer removed with a scalpel was rinsed 3 times with 9% saline solution and then fixed in 10% neutral buffered formalin of 20 times the volume for 24 hours at room temperature. The skin fixation was to avoid any degree of autolysis or putrefaction during the glucose measurements. The fixed skin was pressed between filter paper sheets to squeeze formalin out. The 'dry' skin (epidermis + dermis) of ~1 mm thickness was cut into a circular shape of ~25 mm diameter and glued onto the cylindrical cell with the stratum corneum layer facing the laser beam. The sample holder was rinsed several times with pure human serum to dispose of the formalin residue.

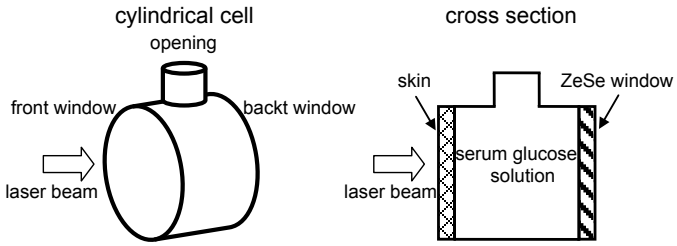

Fig. 3. Schematic diagram of sample holder

4. Results and discussion

4.1. Probing depth in skin

The probing depth (penetration depth) of the photothermal signal is determined by the thermal diffusion length μ_s, that is, the thermal wave amplitude decreases by a factor of e^{-1} within a distance of one thermal diffusion length from the surface. The thermal diffusion length of the modulated signal is given by

$$\mu_s = \sqrt{\frac{\alpha}{\pi f}} \tag{5}$$

where α is the thermal diffusivity of the medium and f is the modulation frequency. In the skin epidermis layer, the thermal diffusivity changes with water content (from 10% to 60%).

To estimate the detection depth in epidermis, two boundary thermal diffusivity values at water content 10% and 60% in the epidermis layer were used in the calculation, $\alpha = 2\text{x}10^{-4}$ cm^2s^{-1} for the human epidermis of thickness ~13 μm as the lower limit [40], and $\alpha = 7\text{x}10^{-4}\text{cm}^2\text{s}^{-1}$ of human epidermis of 260 μm thickness as the upper limit [41]. The real probing depth must be within the two boundaries. Figure 4 displays the modulation frequency dependence of the two thermal diffusion length limits. With 90 Hz modulation frequency used in this study, the probing depth in the skin is between 8.4 μm and 15.7 μm, barely outside the stratum corneum layer. Therefore, 90 Hz is not an optimal frequency, yielding too shallow a

#173338 - $15.00 USD Received 26 Jul 2012; revised 14 Oct 2012; accepted 23 Oct 2012; pub. 29 Oct 2012

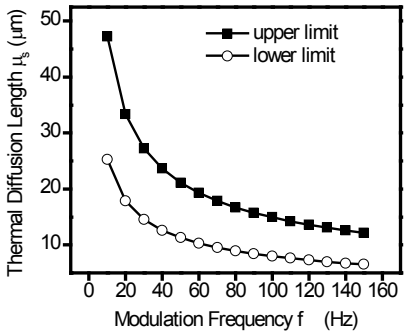

Fig. 4. Modulation frequency dependence of thermal diffusion length in skin. The upper limit of thermal diffusion length is calculated from the thermal diffusivity of epidermis of 260 μm thickness while the lower limit is calculated from the thermal diffusivity of superficial layer of epidermis of 13 μm thickness.

penetration depth. To increase the probing depth, the modulation frequency should be decreased, however, with the current QCLs, the selection of modulation frequency is restricted by the laser output stability.

4.2. Glucose measurements

To ensure the glucose concentration within the skin epidermis layer reached equilibrium with the solution in the cylindrical sample holder after refill of new serum-glucose solution, there was a waiting time of 25 minutes (1500 seconds) with both lasers on before each measurement started. Figure 5 shows a time scan of the differential signals from 280 mg/dl solution immediately after the sample refill. The amplitude ratio *R*, defined as the ratio of serum PTR amplitudes generated from laser A and laser B alone $R = A_{AS} / A_{BS}$, was set at 1.09 by adjusting the laser intensity ratio through the circular variable ND filter in front of laser B. The phase shift *dP*, defined as the phase difference between the pure serum signals $dP = P_{AS} - P_{BS}$, was set at 180.1° by adjusting the waveform modulation phase of laser B relative to that of laser A through the phase-locked function generator. It is seen that both amplitude, Fig. 5(a), and phase, Fig. 5(b) become stabilized after 1500 seconds.

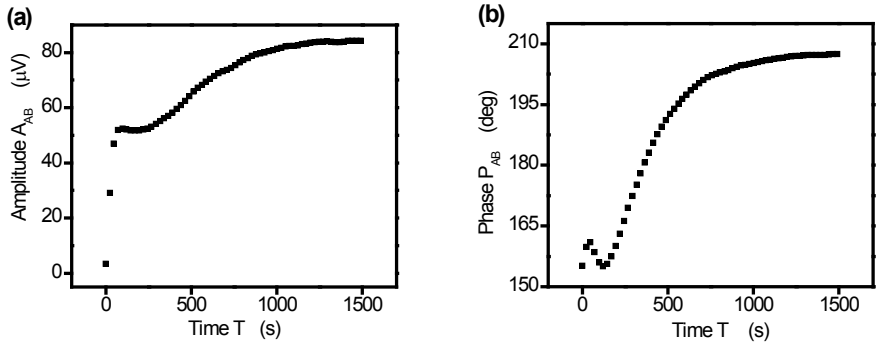

Fig. 5. Time scan of differential signals from 280 mg/dl solution with amplitude ratio *R* = 1.1, phase shift *dP* = 180.1° at 90 Hz. (a) Amplitude; (b) Phase.

Figure 6 displays the amplitude ratio scan (*R* = 0.91–1.09) of WM-DPTR signals with two extreme glucose concentrations, 25 mg/dl and 280 mg/dl. The selection of amplitude ratio scan range is based on the optimal amplitude ratio of the mathematical water-glucose model (R = 0.97 – 1.03) [34] but with an enlarged range (R = 0.91 – 1.09) to include a possibly different optimal amplitude ratio for skin. The amplitude with different glucose concentrations

#173338 - $15.00 USD Received 26 Jul 2012; revised 14 Oct 2012; accepted 23 Oct 2012; pub. 29 Oct 2012

is distributed differently along the amplitude ratio *R*, Fig. 6(a). The V-shape distribution of the higher glucose concentration has a higher curvature and a base at $R < 1$, whereas the distribution of the lower glucose concentration shows a broader V-curve with minimum located at $R \sim 1$. The phase distribution of the two glucose concentrations exhibits large variation, Fig. 6(b). While the phase of the higher glucose concentration experiences a gradual transition from 358° toward 207°, the phase of the lower glucose concentration changes slowly from –26° to 156°. The phase flip-over appeared because the phase shift *dP* was close to, but larger than, 180°, as previously discussed [34]. Figure 6 implies that the most glucose sensitive region where signals differ most in terms of amplitude ratio, is $R > 1$ for amplitude and $R < 1$ for phase. In practice, the selection of optimal amplitude ratio *R* should take signal monotonicity and linearity into consideration.

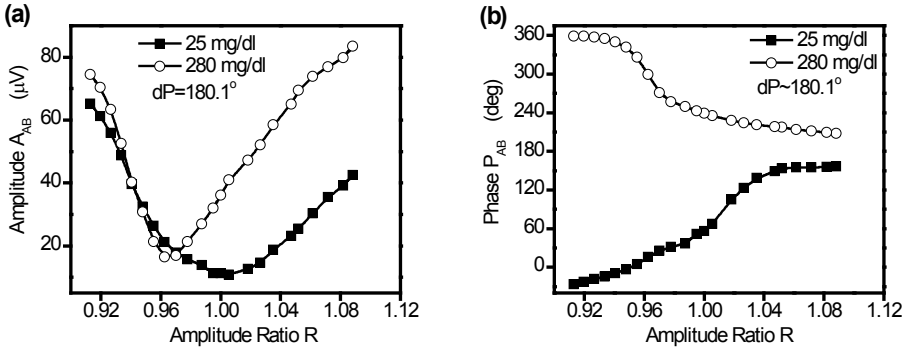

Fig. 6. Signal vs. amplitude ratio R with glucose concentration 25 mg/dl and 280 mg/dl and phase shift dP = 180.1°. (a) Amplitude; (b) Phase.

Figure 7 shows the signal response to glucose concentration change in skin from 25 mg/dl to 280 mg/dl with amplitude ratio $R = 1.00$ for amplitude and $R = 1.09$ for phase. With the optimal *R-dP* combinations, (1.00, 180.1°) for amplitude and (1.09, 180.1°) for phase, both amplitude and phase are monotonic with glucose concentration, with amplitude being more sensitive at high concentrations and phase being more sensitive at low concentrations. When glucose concentration increases from 25 mg/dl to 280 mg/dl, amplitude increases by ~22% (from 11.2 μV to 36.2 μV) and phase increases by 51° (from 156° to 207°).

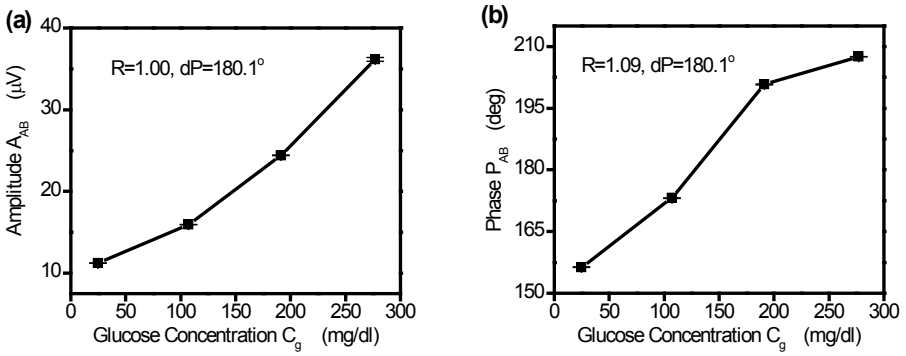

Fig. 7. Signal vs. glucose concentration with different *R-dP* combinations at 90 Hz. The symbols are data points and the lines are a guide to the eye. Error bars were obtained from five measurements. (a) Amplitude; (b) Phase.

Figure 8 presents the signal response in a larger glucose concentration range, from 22 mg/dl to 400 mg/dl with *R-dP* combinations (0.91, 179°) for amplitude, Fig. 8(a) and (0.97, 179°) for phase Fig. 8(b). It can be seen that these combinations favor sensitivity to higher glucose concentrations. Figure 9 exhibits the signal change with glucose in the lower

#173338 - $15.00 USD Received 26 Jul 2012; revised 14 Oct 2012; accepted 23 Oct 2012; pub. 29 Oct 2012

concentration range (21 mg/dl to 130 mg/dl) with *R-dP* combinations (1.04, 174.2°) for amplitude, Fig. 9(a) and (1.09, 174.2°) for phase Fig. 9(b). With these combinations the glucose concentrations with ~37 mg/dl interval are extremely well resolved.

Compared with other noninvasive MIR techniques which have shown encouraging results [24,26,30], together with our previous results [35], WM-DPTR clearly demonstrates superior performance, especially in the low glucose concentration range. Accurate hypoglycemia sensing has always been a challenge in noninvasive glucose monitoring.

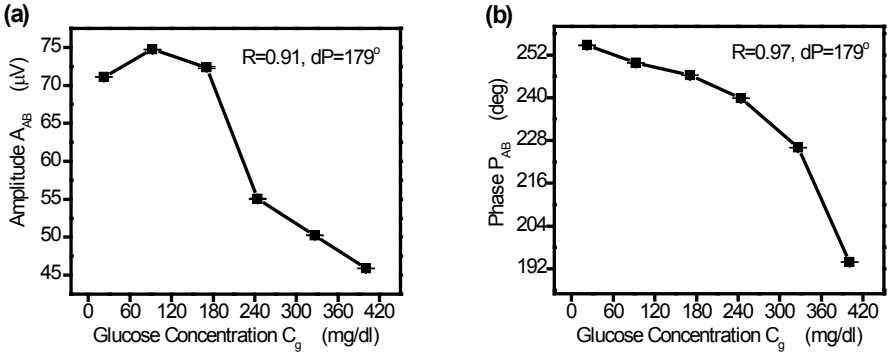

Fig. 8. Signal vs. glucose concentration (22 mg/dl to 400 mg/dl) with different *R-dP* combinations at 90 Hz. The symbols are data points and the lines are a guide to the eye. Error bars were obtained from five measurements. (a) Amplitude; (b) Phase.

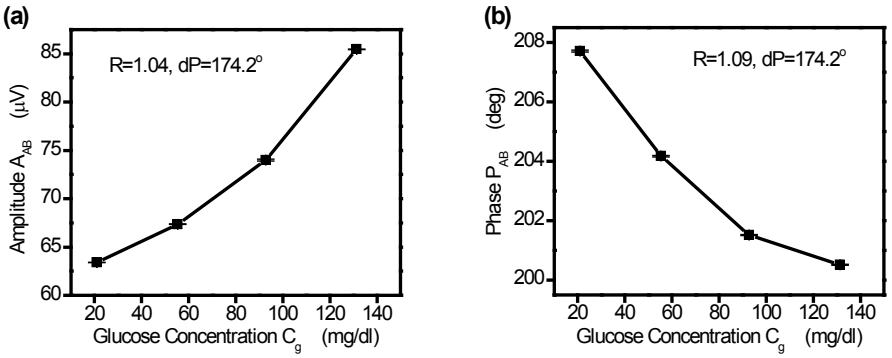

Fig. 9. Signal vs. glucose concentration in low glucose concentration range (21 mg/dl to130 mg/dl) with different *R-dP* combinations at 90 Hz. The symbols are data points and the lines are a guide to the eye. Error bars were obtained from five measurements. (a) Amplitude; (b) Phase.

5. Conclusions

We have reported preliminary in vitro serum glucose measurements in human skin using WM-DPTR. The measurement results in the physiological range (21 mg/dl – 400 mg/dl) demonstrate that WM-DPTR can be used to detect glucose diffused into human skin with high sensitivity. The results also exhibit the tunability of the sensitivity of the WM-DPTRtechnique with two important parameters, amplitude ratio *R* and phase difference *dP* which are controlled by the laser intensity ratio and the modulation phases. The application of WM-DPTR to in vitro glucose detection in serum diffused in human skin sets a solid feasibility base for future in vivo noninvasive glucose detection in a clinical setting as well as for eventual personalized diabetes care. The latter is expected to materialize as CW-QCL prices decrease by 1–2 orders of magnitude and size shrinks to that of a portable laptop, as forecast by the QCL manufacturing industry [42].

#173338 - $15.00 USD Received 26 Jul 2012; revised 14 Oct 2012; accepted 23 Oct 2012; pub. 29 Oct 2012

Acknowledgments

The support of the NSERC-CIHR CHRP program, the Ontario Ministry of Research and Innovation (MRI) through the Premier's Inaugural Discovery Award to AM and of the ORF program, and the Canada Foundation for Innovation (CFI) are gratefully acknowledged. Special thanks to Dr.Trover M. Born at the Toronto Institute of Aesthetic Plastic Surgery for providing us with human skin samples used in the in vitro measurements. We are grateful to Pranalytica Inc. for helpful discussions on, and partial support of, the QCL system.

#173338 - $15.00 USD Received 26 Jul 2012; revised 14 Oct 2012; accepted 23 Oct 2012; pub. 29 Oct 2012